RSC Advances

PAPER

View Article Online
View Journal | View Issue

Cite this: *RSC Adv.*, 2025, **15**, 8719

Removal of protonic doping from PEDOT:PSS by weak base for improving aluminum solid electrolytic capacitor performance†

Piao Luo,[a] Kai Zhang, *[ab] Nanjie Wu,[a] Lanlan Wei,[b] Shigui Peng, [a] Qiao Fan,[a] Tingting Luo,[a] Yucheng Yin,[b] Xiang Zhang,[b] Yufei Liu,[a] Min He,[ab] Jie Yu[ab] and Shuhao Qin [ab]

Received 6th January 2025
Accepted 11th March 2025

DOI: 10.1039/d5ra00124b

rsc.li/rsc-advances

Poly(3,4-ethylenedioxythiophene):poly(styrenesulfonate) (PEDOT:PSS) is a promising conductive polymer material, but its acidic nature leads to device deterioration and poor long-term durability. It is usual practice to neutralise PEDOT:PSS solutions with bases, resulting in a decrease of conductivity. The causes of the decline in conductivity remain disputed and uncertain. In this study, three bases (sodium hydroxide, ammonium hydroxide, and imidazole) were employed to treat PEDOT:PSS to investigate their effects on doping level, composition, and structure. The results show that bases may dedope PEDOT:PSS by removing the proton doping from the PEDOT chain. Meanwhile, insulating PSS is removed, and the aggregated structure is optimised to ensure that conductivity is not significantly reduced. The PEDOT:PSS treated with the weak base imidazole showed the least loss of conductivity due to only a modest decrease in doping level and the greatest loss of insulating PSS. Aluminium electrolytic capacitors made using imidazole pH-adjusted solutions have a capacitance ratio of up to 98.28% and an equivalent series resistance of 26 mΩ. These findings provide a valuable reference for developing high electrical characteristics and neutral PEDOT:PSS materials.

1. Introduction

Poly(3,4-ethylenedioxythiophene):poly(styrenesulfonate) (PEDOT:PSS) is widely used in applications such as capacitors,[1,2] solar cells,[3–5] thermo-electric devices,[6–8] conductive hydrogels,[9–11] and sensors,[12–14] owing to its outstanding electrical conductivity, high transparency, remarkable environmental stability, good film-forming and solution-processability. However, the acidity of PEDOT:PSS solution could cause the device to corrode and affect its normal use. The PEDOT:PSS aqueous solution is a strong acid with pH < 2.5. For example, the pH for widely used commercial Clevios™ PH 1000 (from Heraeus) is 1.5–2.5.[15] For that reason, it is necessary for the acidic PEDOT:PSS solutions to be reduced in acidity, aiming to mitigate against device degradation and prolong service life.

A common route to neutralise the acidic PEDOT:PSS is base treatment. In the last decade, strong bases such as NaOH,[16] KOH,[17] LiOH[18] and guanidine[19] have been used to neutralise acidic PEDOT:PSS solutions effectively. However, this is accompanied by a significant drop in conductivity. In addition, the neutralised solutions were also prepared by treatment of mild bases, ammonium hydroxide and imidazole.[20,21] For instance, Hsieh *et al.*[20] used ammonia to modify the PEDOT:PSS film, then enhanced the surface polarity of the PEDOT:PSS film and inhibited the degradation at the PEDOT:PSS/ITO layer interface. Kim *et al.*[21] used imidazole to neutralise PEDOT:PSS and enhance compatibility between PEDOT:PSS and metal nanowires in transparent conducting electrodes. Mild bases not only could neutralise the inherent acidity of PEDOT:PSS, but also improve compatibility and device efficiency. But there is a lack of comprehensive study on weak bases treatment of PEDOT:PSS characteristics, including doping states, especially for composition and structure, which are critical for electrical properties.

In general, the electrical conductivity of a conducting polymer is related to its carrier concentration and carrier mobility. Carriers in doped conductive polymers exist in the form of polarons or bipolarons. Polarons were generated by adding or removing electrons from the conjugated chains, and then bipolarons were formed by the combination of two polarons with the same charge.[22,23] It has been widely reported that PEDOT is doped by oxidation of the oxidant itself during the polymerisation process to achieve p-type doping, thereby generating carriers and enabling the PEDOT chain to conduct electricity.[23] It is commonly admitted that the carrier

[a]*Department of Polymer Material and Engineering, College of Materials and Metallurgy, Guizhou University, Guiyang, China. E-mail: k.zhang2008@qq.com*
[b]*National Engineering Research Center for Compounding and Modification of Polymeric Materials, Guiyang, China*

† Electronic supplementary information (ESI) available. See DOI: https://doi.org/10.1039/d5ra00124b

concentration is related to the doping level, while the carrier mobility is associated with the degree of order and relative stacking between the PEDOT chains, and high-efficiency intra- and inter-chain transport can optimise the carrier mobility.[12,24] As mentioned above, the electrical properties of PEDOT:PSS could be influenced by the treatment of bases.[25–28] It has been partially shown that base treatment reduces the doping level, decreasing the carrier concentration. For example, Chin *et al.*[29] added sodium hydroxide to the PEDOT:PSS solution and discovered the hydroxide ions provided by the base deprotonated the acidic sulfonates, which reduced the stability of polarons and bipolarons on the doped thiophene to achieve de-doping. The same argument was applied in most relevant reports, but there exist different views. Yao *et al.*[30] reported that the NaOH treatment can dedope PEDOT:OTf directly by removing the protonic acid doping, which differs from the mechanism for de-doping of reductants, but this is not the focus of the study. Additionally, base treatment could alter the composition and structure of PEDOT:PSS, which affects carrier mobility. Heeger and co-workers[31] reported base treatment would increase the pH of PEDOT:PSS, causing an increased distance between conducting clusters. Kong *et al.*[27] found that the surface morphology change of base treatment was to be dramatic, which affected the size of the PEDOT particles, resulting in less readily charge transport. Abundant work has shown the main reason for the drop in conductivity that bases addition induces the decline of carrier concentration, it is clear that bases such as NaOH cannot serve as reducing agents to dedope oxidized(doped) PEDOT.[26] The essential reason for the drop in carrier concentration is still unclear, so there is still a significant and challenging task to explore the explanation for the decrease of carrier concentration. At the same time, there is still no systematic explanation for whether base without reducibility can dedope PEDOT directly. Researchers typically use bases with almost no redox properties to adjust the pH of PEDOT:PSS solutions, such as sodium hydroxide (NaOH), ammonium hydroxide (NH_4OH), and imidazole (IM). Among these, sodium hydroxide and ammonium hydroxide are inorganic bases, while imidazole is an organic base, each exhibiting different alkalinity. We attempt to investigate the influence and differences in the strength and composition of these three bases on the properties of the treated PEDOT:PSS materials and the performance of solid electrolytic capacitors.

In this work, the effects of PEDOT:PSS film on doping level, composition and structure were systematically investigated by treatment with three bases. These three different bases (NaOH, NH_4OH, IM) have weak redox properties generally. An attempt was made to clarify the effect of base treatment on carrier concentration and carrier mobility and its mechanism. The results indicate that base treatment would change carrier concentration, causing lower conductivity, potentially. Nevertheless, base treatment also removes insulating PSS effectively and optimises the aggregated structure at the same time, leading to an increase in carrier mobility. Among the three bases, imidazole showed a slight drop in carrier concentration and an increase in carrier mobility with neutralisation of the PEDOT:PSS solution. The treatment with mild base imidazole achieved minimised loss of electrical conductivity of PEDOT:PSS and enhanced the electrical performance of aluminium electrolytic capacitors finally. The method and conclusions of the experiment greatly contribute to the theoretical foundation for the creation of low-corrosion, highly conductive PEDOT:PSS materials.

2. Experimental

2.1 Materials

3,4-Ethylenedioxythiophene (EDOT), sodium persulfate, iron sulfate, dimethylsulfoxide (DMSO), sodium hydroxide, ammonia (25–28%), and imidazole were purchased from Aladdin; PSS ($M_w \sim 75\,000$, 30 wt% in H_2O) was purchased from Macklin, and ethanol absolute was purchased from Tianjin Fuyu Fine Chemical Co.

2.2 Synthesis and treatment of PEDOT:PSS and aluminium solid electrolytic capacitors

The initial dispersion was obtained by adding EDOT to a mixed solution of deoxygenated sodium persulfate, iron sulfate and sodium polystyrene sulfonate, then stirring the solution in a vacuum atmosphere at 10 °C for 24 h. After the reaction, ion exchange resin was added to carry out the ion exchange, and the dispersion was filtered by stirring for 6 h to obtain the PEDOT:PSS dispersion. Then add 5% DMSO to dope and spin-coat at 2000 rpm for 40 s to obtain a uniform film, and finally anneal the film on a hot plate at 110 °C for 20 min. 500 μL of 1 mol L^{-1} base solution was dropped on the PEDOT:PSS film at room temperature and left in air for 5 min, then the glass slide with the film was soaked in 5 mL of anhydrous ethanol for 10 min to remove the residual base. The treatment of the film was repeated for a total of 5 times and placed on a hot plate at 110 °C for 20 min to dry. When performing the second acid treatment, the molar concentration of the dilute sulfuric acid solution used is 1 mol L^{-1}.

Solid aluminium electrolytic capacitors with a wire-wound core made by Guizhou Yunrui, rated voltage and capacitance were 25 V and 470 μF, respectively. PEDOT:PSS aluminium solid electrolytic capacitors were successfully prepared by immersing the wire-wound components in pH-adjusted aqueous dispersions of PEDOT:PSS using different bases under high vacuum for 30 min, drying at 150 °C for 30 min, repeating the procedure three times, and then casing the capacitors.

2.3 Characterisation

The conductivity of PEDOT:PSS films was measured by using FT-330 four-point probe instrument, and the film thickness was tested with a Carl Zeiss LSM900 laser confocal microscope. Absorption spectra were studied in the range of 2500–200 nm using a Shimadzu UV-3600i Plus UV-Vis-NIR spectrometer. Electron paramagnetic resonance spectroscopy (EPR) was recorded on a Bruker EMXplus-6/1 X-band spectrometer. Raman spectra were obtained using a HORIBA LabRAM Odyssey Raman Spectroscopy Imager, using a laser with a wavelength of 532 nm as the excitation source. Measurement of Fourier

Transform Infrared Spectroscopy (FTIR) of thin films in the range of 400 to 4000 cm^{-1} was conducted on a Nicolet IS50 FT-IR spectrometer. X-ray photoelectron spectroscopy (XPS) of thin films was acquired using a Thermo ESCALAB 250Xi X-ray photoelectron spectrometer equipped with an Al Kα X-ray source. Atomic force microscopy (AFM) images were acquired in tap mode using a Bruker Dimension Icon atomic force microscope. For grazing incidence wide-angle X-ray scattering (GIWAXS) measurements, a GIWAXS instrument (Xeuss 2.0) and a Pilatus 3R 300K detector from Xenocs were used. The carrier concentration and carrier mobility of the films were measured using an Ecopia HMS-7000 Hall effect tester. The TH 2826 LCR meter (Jiangsu Tonghui Electronics Co., Ltd.) was used to measure the lead-in capacitance, dielectric loss tangent (tg δ) and equivalent series resistance (ESR) at different frequencies. The cyclic voltammograms and galvanostatic charge/discharge curves were characterized on an electrochemical workstation (CHI760F, China), measured in a voltage range of 0–1 V at scan rates of 50 mV s^{-1} and current densities of 1 A g^{-1}, respectively.

3. Results and discussion

3.1 Doping level

UV-vis-IR spectroscopy can be utilised to probe doping level changes that occur in the conjugated polymers.[32] The treatment of PEDOT:PSS films by bases was studied by UV-is-NIR absorption spectroscopy. There are three doping states of PEDOT, namely $PEDOT^{2+}$ (bipolaron), $PEDOT^{+}$ (polaron), and PEDOT (neutral), which can be detected by the characteristic absorptions at 1400 nm (bipolaron), 900 nm (polar), and 500 nm (neutral state).[33] The doping level can be considered as the strength of the charge carriers, and bipolarons tend to appear on PEDOT chains with high doping levels.[24,32] As shown in Fig. 1(a), the absorption at 400–600 nm and 800–1000 nm is significantly enhanced after base treatment, and the absorption at 1400 nm is reduced, suggesting that the base treatment can decrease bipolarons. Among the three bases, the NH_4OH and IM treatment films behave similarly, while the film of NaOH treatment shows a stronger change. Even a pronounced increase in absorption at 500 nm is observed after NaOH treatment, implying the occurrence of neutral state induced by the NaOH treatment, while the NH_4OH and IM treatments hardly affect this band. The absorption at 1400 nm of the NH_4OH treatment sample is not significantly different from the treatment of IM, while the NH_4OH treatment marginally enhances the absorption band at 800–1000 nm. This evolution of bipolarons and neutral states after base treatment indicates a decrease in the quantity of charge carriers. In other words, this suggests a reduction in the doping level.

Electron paramagnetic resonance (EPR) is a valuable technique for distinguishing radicals from diradicals, because radicals (such as polarons) have a spin of $\frac{1}{2}$ and can be identified, whereas diradicals (such as bipolarons) possess an integer spin and cannot be recognised in EPR.[34,35] Then the samples were further studied by EPR, which probed the population of polarons. As shown in the Fig. 1(b), the PEDOT:PSS samples exhibit an intense single-line EPR signal with a *g*-factor of 2.0033, which is typical of free non-spin-paired electrons delocalised across the conjugated π-system.[36] The stronger EPR signals of NaOH-treated PEDOT:PSS films indicated more polarons in PEDOT chains. The population of radicals was calculated by double integrating of the EPR intensity and normalising the integrated value to the PEDOT percentage of

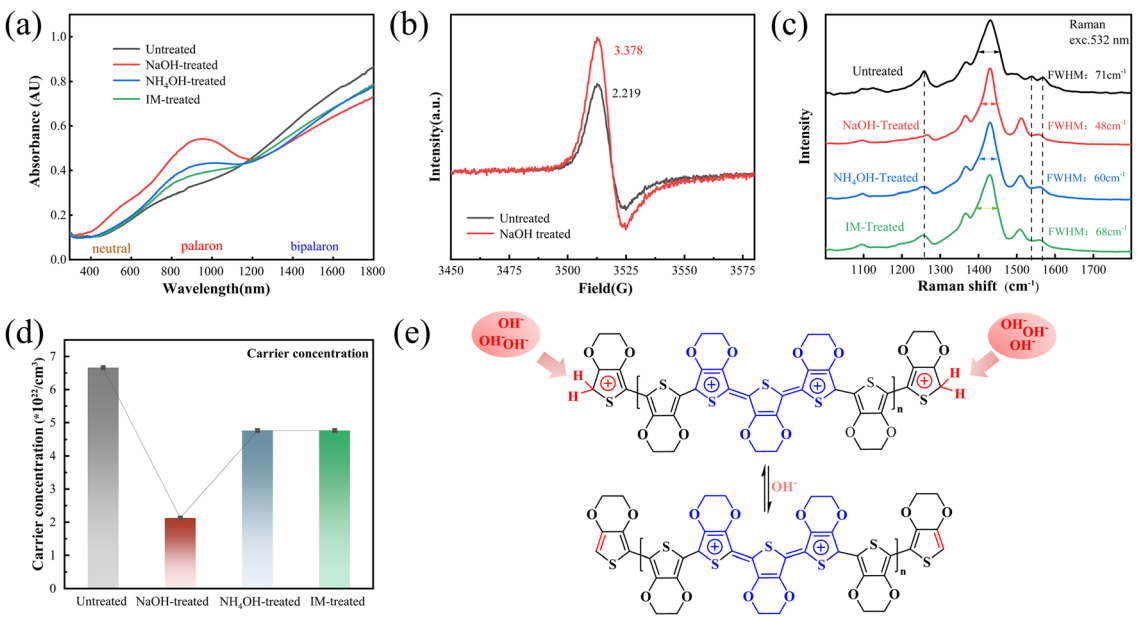

Fig. 1 (a) The UV-vis-NIR absorption spectra of untreated and base-treated PEDOT:PSS films. (b) Electron paramagnetic resonance spectra of the PEDOT:PSS of untreated and NaOH treated. (c) Raman spectra of PEDOT:PSS of untreated and treated with bases measured at a 532 nm laser (d) Carrier concentration of different films were tested by Hall effect. (e) Proposed dedoping mechanism of base without redox properties.

sample weight, because base treatment may remove PSS. The double integrated EPR intensity increases from 2.219 to 3.378 with treatment of NaOH. This indicates increased polarons in the PEDOT:PSS, in agreement with results of UV-vis-NIR absorption spectroscopy. The bipolaron may be converted to polaron, leading to an increase of polaron concentration.[37] There is a transformation of PEDOT from a high doping level to a low doping level after treatment with bases.

The Raman spectrum provides detailed information about the structural transformation of PEDOT depending on the doping level, which reveals the vibrational modes of PEDOT.[38,39] The Raman signals between 1400–1500 cm^{-1} originate from the C_α=C_β telescopic vibration. In addition, other characteristic peaks correspond to the asymmetric C_α=C_β bending at the chain's terminal thiophene rings (1571 cm^{-1}), asymmetric C_α=C_β bending splitting (1537 cm^{-1}), asymmetric C_α=C_β bending in the middle of the chain (1504 cm^{-1}), C_β–C_β stretching (1370 cm^{-1}), and C_α–C_α' inter-ring stretching (1271 cm^{-1}).[40] As depicted in Fig. 1(c), the strongest band at 1431 cm^{-1} narrows and moves to 1429 cm^{-1} following the base treatment of PEDOT:PSS films. Additionally, it is clearly narrower after being treated with sodium hydroxide. The strongest band shows a half width at half maximum (HWHM) of 71 cm^{-1} for the untreated PEDOT:PSS sample. However, the PEDOT:PSS film with NaOH, NH_4OH, IM treatment display a HWHM values of 48 cm^{-1}, 60 cm^{-1}, and 68 cm^{-1} respectively. This can be ascribed mainly to the conformational change of PEDOT induced by dedoping.[41] Moreover, the intensity of the peak at 1504 cm^{-1} was significantly enhanced and shifted to 1511 cm^{-1}, the peak at 1537 cm^{-1} disappeared, and the intensity of the peak at 1571 cm^{-1} was weakened and shifted to 1560 cm^{-1} after treatment of three bases. The peak at 1271 cm^{-1} with the intensity weakened and shifted to higher wave numbers. These changes are similar to those observation from other reports for PEDOT:PSS films were reduced by the chemical reducer hydrazine and electrochemically.[42,43] There is a phenomenon similar to de-doping by reduction of oxidised PEDOT. But it is usually considered that NaOH, NH_4OH and IM cannot act as reducing agents to reduce the oxidised state of PEDOT, other non-redox dedoping mechanisms should be operative in this case. The peak at 1266 cm^{-1} in the infrared spectra as shown in Fig. S1 (ESI†) representing the C_α–C_α' interring stretching was red-shifted to 1255 cm^{-1} after bases treatment, which also indicates a reduction in the level of doping.[44]

There is a transformation from bipolarons to polarons and from conducting states to neutral states, as well as a decrease in the doping level. This all affects the carrier concentration to some extent. The carrier concentration of the four PEDOT:PSS samples was obtained with the Hall effect. As expected, the carrier concentration remarkably decreases after base treatment of PEDOT:PSS films as shown in Fig. 1(d). The lower the doping level inferred by observation of UV-vis-NIR and Raman spectra, the lower the carrier concentration. After treatment with NaOH, the sample is supposed to have the lowest doping state, and there is a significant drop in the carrier concentration (68%), and it is decreased only 29 percent with treatment of weak base ammonia and imidazole.

The more probable reason for dedoping is the deprotonation of initially heavily protonated PEDOT chains. Previous study has demonstrated that the thiophene ring's C_α protonation in PEDOT chain end groups.[45] EDOT oligomers have also been shown to be protonated in the presence of trifluoromethanesulfonic acid, trifluoroacetic acid, *etc.*, and the UV spectra of the protonated material have a significant red shift.[46] A protonation would be equivalent to introducing a positive charge in the π-system, *i.e.*, equivalent to an oxidation.[37] The proposed mechanism of PEDOT:PSS dedoping by bases without redox properties is illustrated in Fig. 1(e). There are many end groups since PEDOT chains are commonly thought to have a low molecular weight and only include 10–20 monomer units.[47] Consequently, these bases treatment can significantly affect the doping level by removing protonic acid doping of a large number of end groups, then reducing the carrier concentration. It remains to be studied whether the presence of protonation exists in the intermediate chain segment of PEDOT or not.

The different levels of de-doping caused by the three bases may be due to the different ability of deprotonation and thus different carrier concentrations. The basicity constant (pK_b), is an intrinsic property of bases that quantifies the ability to bind with protons.[48,49] For instance, a lower or negative pK_b value suggests that bases are more basic and have a greater ability to bind protons. It is well acknowledged that the three bases exhibit different pK_b values, NaOH exhibits the lowest pK_b values, and NH_4OH has middle pK_b values, while IM displays the highest pK_b values, respectively. The lowest doping level of the PEDOT:PSS films with NaOH treatment can be attributed to the strongest ability of deprotonation.

A second treatment with dilute sulfuric acid was applied to the NaOH-treated films. The acid retreatment cannot further decrease the PSS content, but partially recover the doping level, characterised by UV-vis-NIR spectroscopy, Raman spectra and ATR-FTIR spectra, as shown in Fig. S2.† These reversible transformations further suggest that the reduction in doping levels is probably owing to the removal of PEDOT protons.

3.2 Composition and structure

The composition and structure of conductive polymer materials have a significant impact on their intrinsic properties. Furthermore, the results show that base treatment also influences the composition and structure of the polymer and influences the carrier mobility. PEDOT:PSS exhibits a core–shell structure, with the hydrophilic and insulating PSS shell enclosing the hydrophobic and conductive PEDOT.[50] In the composite system composed of PEDOT and PSS, PSS (polystyrene sulfonic acid) is typically regarded as an insulating material. As a result, the structure and characteristics of PEDOT:PSS are significantly influenced by the PSS content. In order to determine the PSS content of films, we systematically characterised the PEDOT:PSS films of untreated and base-treated films. Fig. 2(a) shows the UV-vis-NIR absorption spectra of untreated and three bases treatments, respectively. The absorption band at 226 nm was ascribed to the aromatic

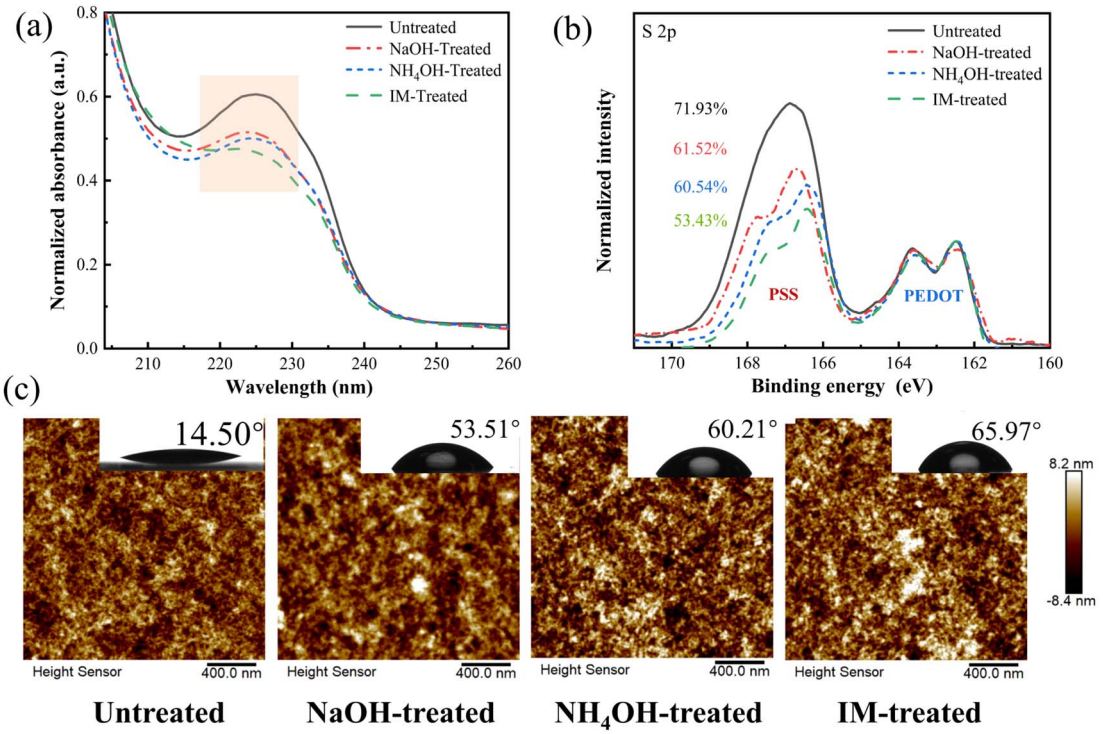

Fig. 2 (a) The UV-vis-NIR absorption spectra (b) S 2p XPS spectra of the untreated, base-treated PEDOT:PSS films. (c) AFM height images of various films and contact angles of water droplets on PEDOT:PSS films are in the upper right corner. The size of all AFM images is 2 × 2 μm.

ring of PSS,[33] and the intensity of the peak at 226 nm decreased significantly after base treatments. The loss of poly(4-styrenesulfonic acid) (PSS) on the PEDOT:PSS film with base treatments was evidenced by the decrease in its intensity. When bases are added, PSSH is changed into salts like PSSNa, $PSSNH_4$, *etc.*, which destroys the Coulomb force between PEDOT and PSS and results in phase separations, making it easy to remove PSS. Among the three bases, imidazole aqueous solution removed the most PSS, followed by ammonia, and sodium hydroxide solution treatment removed the least amount. This could be explained by the fact that imidazole's large molecular size can cause steric hindrance and weaken the interaction force between PEDOT and PSS, leading to a more readily PSS removal from PEDOT:PSS films.

To further ascertain the lost PSS content, the films were detected by XPS, and the results are shown in Fig. 2(b). The S(2p) signals of the sulfonate group of PSS (167–171 eV) and the thiophene unit of PEDOT (163–167 eV) are distinguished based on their different chemical environments. The S(2p) electrons in the sulfonic acid group exhibit higher binding energy due to the presence of three electronegative oxygen atoms.[51] After bases treatment, the peak at 167 eV was significantly reduced due to the removal of PSS, and the imidazole-treated film also experienced a significant decrease in peak intensity. The peak intensity at 164 eV represented thiophene sulphur on PEDOT and remained virtually constant. The untreated film had 71.93% PSS content after XPS peak area integration. The base treatment decreased the PSS content by 10–20%, with ammonia and imidazole treatments lowering it to 60.54% and 53.43%, respectively, and sodium hydroxide treatment lowering it to 61.52%. The result of XPS was consistent with the UV-vis-NIR spectroscopy. At the same time, the hydrophilicity of the film surface and the bright and dark distribution states of the AFM (atomic force microscopy) height map are likewise influenced by the PSS content. Following the removal of the hydrophilic PSS, the film's water contact angle rises, as seen in Fig. 2(c). Additionally, the AFM image shows a decrease in the distribution of the PSS's dark phase.[50] From the topographic images (Fig. S3a†) of the 2 μm × 2 μm scanned region it was observed that before base treatment the surface was significantly smoother. Upon three base treatments, the surface became slightly rough. The surface of the film after base treatment shows significant height variations and more bright particles, whereas the untreated film surface remains relatively uniform. From the surface height profiles (Fig. S3b†) it was observed that before base treatment the surface was smooth (the vertical fluctuations of data points were ±0.5 nm) and became relatively rough after base treatment (fluctuations of ±2 nm). The insulating PSS phase is partially removed after base treatment, and the reduction of the insulating component can favour carrier transport theoretically.

As mentioned above, the elemental analysis and constituent distribution suggest that partial PSS was removed effectively, complex structural rearrangements of PEDOT:PSS occur at the same time. The structural changes of the PEDOT:PSS films after treatment with bases were detected by AFM further. Comparing a single AFM image under several experimental settings is insufficient to produce definitive conclusions in sub-nanometer

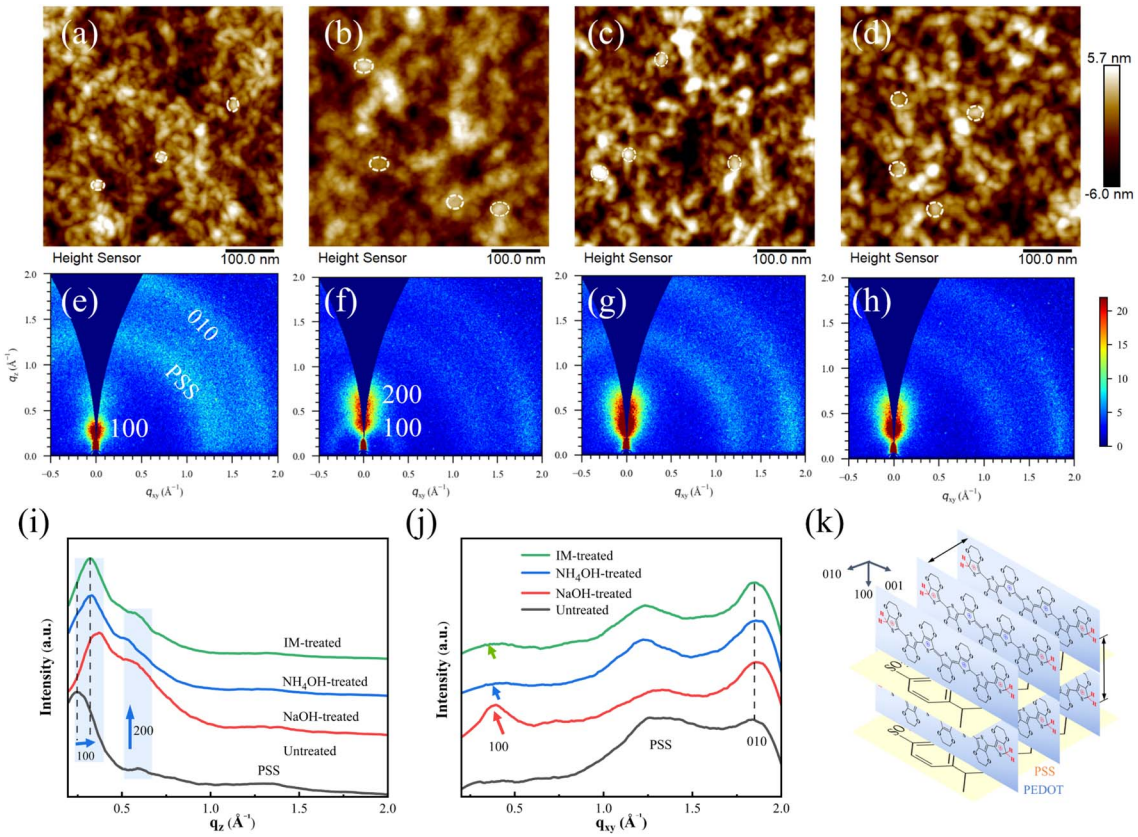

Fig. 3 (a–d) AFM height images of untreated and bases treated PEDOT:PSS films. All the scan areas are: 500 × 500 nm^2. (e–h)2D GIWAXS patterns of the PEDOT:PSS films (e) untreated, and with base (f) NaOH, (g) NH_4OH, (h) IM treated. Linearly offset 1D GIWAXS patterns of various PEDOT:PSS films with (i) out-of-plane (q_z) or (j) in-plane (q_{xy}) scattering geometry. (k) Schematic diagram of the lamellar stacking structures of PEDOT:PSS.

scale study.[52–54] AFM images from 50 distinct locations on the film were collected to statistically analyze the distribution of surface morphology and roughness, thereby reflecting the general trends in surface variations across the film (as can be seen in the Fig. S4†). It was observed that the roughness of the film surface before base treatment was 1.91 nm and its distribution was narrower. Bases treatment will remove the PSS dark phase, causing height differences on the film surface, thereby increasing roughness. The roughness average on the film after bases treatment increased to 2.12 nm, 2.46 nm, 2.30 nm respectively and the distribution widened to a range of 1.90 nm to 5.00 nm. The change in PEDOT grain sizes may be the cause of the roughness increase. Fig. 3(a)–(d) reveal that the PEDOT grain size increased significantly following base treatment, in contrast to the untreated sample. Furthermore, the film treated with NaOH displays the largest PEDOT crystallite domain size, while the size of PEDOT grains is smaller and similar following treatment with weak bases such as imidazole and ammonia. In comparison to the untreated film, these interconnected large grains further increase bright PEDOT-rich domains. The enlarged conducting PEDOT-rich core will reduce charge transport barriers and then enhance carrier mobility.[55] Another reason for increased roughness is that phase separation between PEDOT and PSS, which destroys the surface topography of PEDOT:PSS.[39]

Moreover, the crystal structure at molecular scales of different thin films was tested by using grazing incidence wide-angle X-ray scattering (GIWAXS). GIWAXS is an advanced technique to analyse the molecular packing of PEDOT films.[56] Fig. 3(e)–(h) shows the 2D GIWAXS patterns of the PEDOT:PSS films, where the scattering intensity generally decreases following each of the three base treatments. It's worth noting that the film treatment with weak bases exhibits stronger scattering intensities in comparison with the weaker patterns of the NaOH-treated film. It is reported that the scattering intensities can infer the order of the film crystallinity.[55,57] Therefore, the weak base NH_4OH-treated film displays enhanced crystallinity, followed by the film with imidazole treatment, compared with the NaOH-treated sample. Nevertheless, there is a decrease in crystallinity after all three base treatments. To give a deep insight into the structure change, the 2D GIWAXS pattern was transformed into 1D curves, as depicted in Fig. 3(i) and (j). The peak at 0.27 Å, 0.60 Å in the out-of-plane direction is attributed to PEDOT and PSS laminar stacking (100), (200) reflections, while $q_z = 1.30$ Å corresponds to amorphous PSS.[58] As shown in Fig. 3(i), the alternating stacking peaks (100) of PEDOT and PSS increased from $q = 0.27$ Å ($d = 23.27$ Å, calculated as $d = 2\pi/q$)

to 0.37 Å ($d = 16.98$ Å), 0.32 Å ($d = 19.63$ Å), and 0.31 Å ($d = 20.26$ Å) respectively, after treatment of three bases. The schematic diagram for the molecular packing structure of PEDOT:PSS is displayed in Fig. 3(k). The peak movement made it evident that the base treatment reduces the alternating interlamellar stacking distance between PEDOT lamellae, which improves charge transport along the d100 direction. In addition, a significant increase in the intensity of the 200 peak is observed, which will simplify the charge transfer between adjacent PEDOT chains and thus increase the conductivity.[59] In the in-plane patterns (q_{xy}) (Fig. 3(j)), 0.37 Å, 1.30 Å, 1.85 Å correspond to PEDOT and PSS laminar stacking (100), amorphous PSS and π–π stacking of PEDOT (010).[55,56] Obvious enhancement of the 100 reflection can be observed after NaOH treatment, and the (100) reflection was slightly strengthened by weak bases. The 010 reflection shows no noticeable changes with treatment of bases, indicating the π–π stacking of PEDOT remains unaffected ultimately. But the more closely packed of the PEDOT chains with larger grain sizes along the 100 direction would promote charge transport, it is possible to enhance carrier mobility.

3.3 Conductivity of PEDOT:PSS films

All cases showed a decrease in conductivity after base treatment, but the percentage of decrease was not the same for different base treatments. The results are presented in Table 1. The films treated with ammonia and imidazole solutions had conductivities of 334 S cm^{-1} and 367 S cm^{-1}, respectively, while the films treated with sodium hydroxide had conductivities as low as 247 S cm^{-1}. As previously stated, low doping levels may result in low conductivity, but the removal of insulating components and closer packing of PEDOT chains can favour higher conductivity. The effect of base treatment on the conductivity of PEDOT:PSS films is multifaceted and uncertain. Basically, electrical conductivity is determined by carrier concentration and carrier mobility. The carrier concentration and carrier mobility of bases treated films were measured by the Hall effect. The carrier concentration declined and was consistent with the conductivity's downward trend, while carrier mobility rose. The removal of the insulating PSS and the optimisation of aggregation structure improved the carrier mobility, which can lessen the loss of conductivity caused by the decrease in carrier concentration to a certain extent.[60,61] This is the reason that the conductivity does not decrease significantly after removing proton doping, which drops by several orders of magnitude when treating PEDOT:PSS with a base with reducing properties.[27] Fig. 4 illustrates the changes of PEDOT:PSS films before and after base treatment.

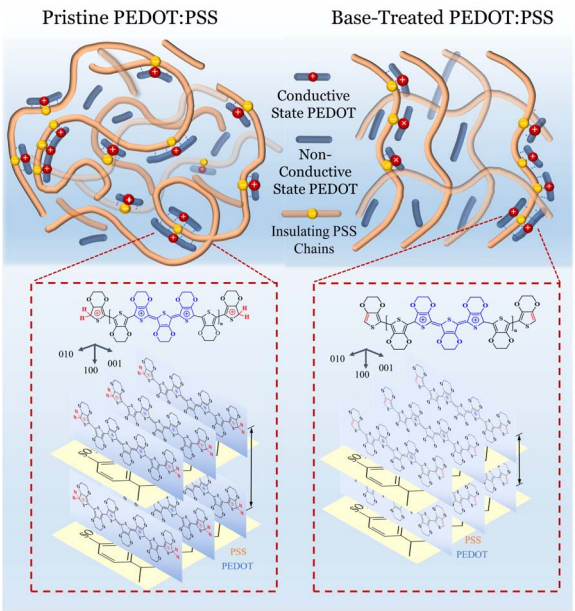

Fig. 4 Schematic illustration for changes of pristine PEDOT:PSS and base treatment PEDOT:PSS.

Conductivity increased and doping levels recovered in the base-treated PEDOT:PSS films after protonation with sulfuric acid again (Fig. S2†). The reversible change is similar to the case of polypyrrole, which is unquestionably proton-doped.[62] However, the conductivity could not be restored to the original level due to the damage to the film surface by the solution post-treatment.

3.4 Electrical performance enhancement of aluminum electrolytic capacitor

Base treatment can suppress the acidic corrosion but does not reduce conductivity significantly. Three bases were employed to tune the pH of the PEDOT:PSS solution, and then we produced winding components of aluminium solid electrolytic capacitors using these PEDOT:PSS water dispersion as the cathode material to investigate the effects of base treatment on the electrical performance of capacitors. As shown in Fig. 5(a), the capacitance ratio obtained from the original PEDOT:PSS dispersion was 88.75%, the maximum capacitance ratio rose to 98.28% after neutralisation using the three bases. The adjustment of pH with bases facilitates the enhancement of the elicited capacitance. The capacitance of an electrolytic capacitor is expressed by the formula $C = \varepsilon S/d$, with ε, S, and d denoting the dielectric

Table 1 Average electrical conductivity, carrier concentration and carrier mobility of PEDOT:PSS

Sample	Average conductivity (S cm^{-1})	Carrier concentration ($\times 10^{22}$ cm^{-3})	Carrier mobility (cm^2 V^{-1} s^{-1})
Untreated	479 ± 31	6.66	0.4855
NaOH-treated	247 ± 35	2.13	0.5806
NH_4OH-treated	334 ± 29	4.76	0.5410
IM-treated	367 ± 27	4.76	0.5426

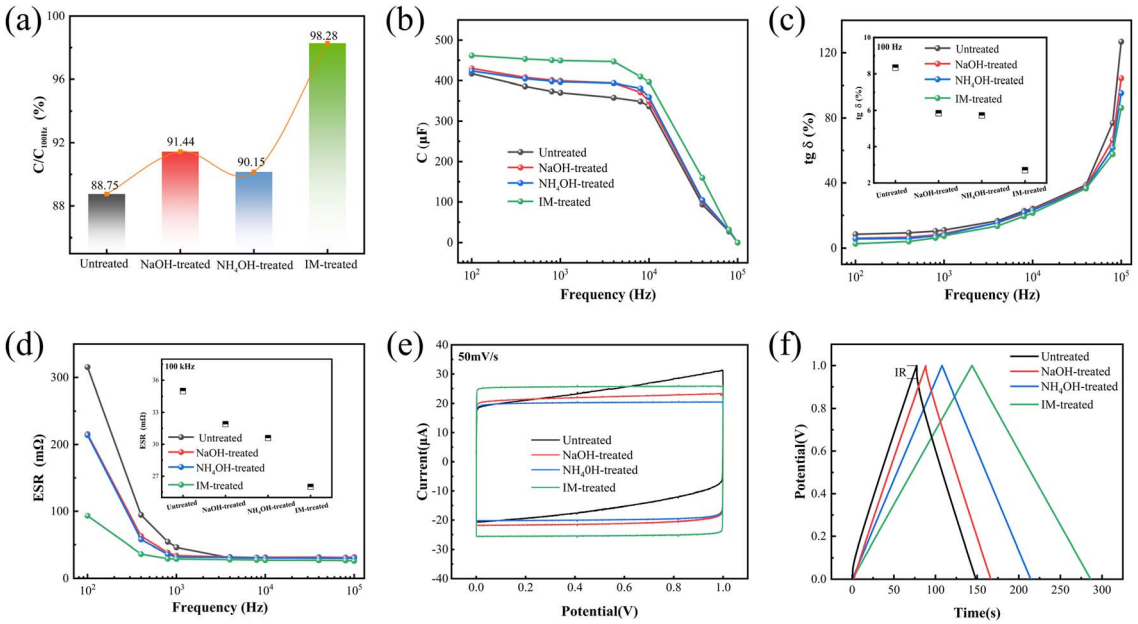

Fig. 5 Electrical characteristics of PEDOT:PSS aluminium solid electrolytic capacitor fabricated using the pristine PEDOT:PSS water dispersions and PEDOT:PSS solution neutralized by different bases as cathode material. (a) The capacitance ratio at 120 Hz; (b) frequency characteristics of capacitance (Cap); (c) frequency characteristics of the dissipation factor (tg δ %); (d) frequency characteristics of equivalent series resistance (ESR); (e) cyclic voltammograms measured at scan rates of 50 mV s^{-1}; (f) galvanostatic charge/discharge curves measured at current densities of 1 A g^{-1}.

constant, electrode surface area, and thickness of the dielectric oxide film, respectively. ε is a constant, the thickness of the dielectric of a wound aluminium capacitor is determined during the manufacturing process and the electrode surface area depends on the effective area of the PEDOT:PSS attached to the porous aluminium foil. The change in capacitance is only related to the effective contact area between the PEDOT:PSS and the anode foil. During the drying process, the liquid cathode in the porous aluminium oxide foil is converted into a solid conductive polymer. The capacitance of the real solid electrolytic capacitor is less than the ideal capacitance because the conductive polymer is unable to completely cover the porous cathode layer. When using a pH-adjusted PEDOT:PSS solution to soak anode aluminium foils, hygroscopicity and acidic corrosion are alleviated because of partial removal of PSS and pH adjustment, which improve the lead capacitance and the stability of the capacitor. As depicted in Fig. 5(b). It was observed that the capacitance that can be extracted under an alternating current decrease with increasing frequency. At high frequencies, the capacitor behaves like a path, and the inductance of the wound aluminium capacitor rapidly increases while the lead capacitance rapidly decreases to zero. But the capacitance of capacitors made from pH-adjusted solutions with three bases is always higher than that of capacitors manufactured from the original PEDOT:PSS dispersion. The imidazole-treated capacitance decreases slowly with increasing frequency. For example, the elicited capacitance at 10 kHz is 84.41%, whereas the elicited capacitance of the electrolytic capacitor made of untreated PEDOT:PSS has fallen to 71.65%. This demonstrates the boosting effect of base treatment on the lead capacitance and capacitance stability.

In an AC circuit, the capacitor must consume a small fraction of the usable signal power. The loss angle tangent (tg δ) is the ratio of active to reactive power used at a sinusoidal voltage of a specific frequency.[63] The equivalent circuit of an electrolytic capacitor is often simplified to a resistance and capacitance in series, with Rs denoted as equivalent series resistance (ESR). After neutralisation with bases, it is seen from Fig. 5(c) and (d) that the aluminium electrolytic capacitors showed a reduction in both loss and equivalent series resistance. The imidazole treatment reduced tg δ from 8.3% to 2.7% at 100 Hz and ESR from 35 mΩ to 26 mΩ at 100 kHz. The increasing pH value by tuning with bases can ease the corrosion of the anode foil and then lower interfacial contact resistance. Hence, bases-treated electrolytic capacitors consistently have better capacitor performance as frequency increases, and capacitors with imidazolium-adjusted pH have the lowest loss and ESR.

To conduct a more thorough assessment of the PEDOT:PSS aluminum solid electrolytic capacitors' performance, cyclic voltammograms (CV) and galvanostatic charge–discharge (GCD) curves were measured. The cyclic voltammograms of sweep rates at 50 mV s^{-1} for all samples are shown in Fig. 5(e). The cyclic voltammograms of base-treated PEDOT:PSS aluminum solid electrolytic capacitor show typical rectangular shapes. The CV curves of pristine capacitor shows a deviation from the quasi-rectangular shape. Moreover, the CV graph of IM-treated capacitor has a larger area, indicating better electrochemical capacitive properties. Fig. 5(f) shows GCD curves of the four PEDOT:PSS capacitor at constant current density of

1 A g^{-1}. The GCD curve of pristine capacitor shows small voltage drop (*IR* drop) at the beginning of discharge curve, result from the higher ESR value of pristine capacitor. The base-treated PEDOT:PSS capacitors present the symmetric and linear charge–discharge behavior and among them IM-treated capacitor have the nearly isosceles triangle shape, indicate the highly reversible and better capacitive behavior of capacitors.

4. Conclusions

In summary, this work provides further insight into the impacts and mechanisms underlying the doping levels, composition, and structure of PEDOT:PSS films upon treatment with bases. It was found that the base without redox properties treatment of PEDOT:PSS may affect the doping level by removing proton doping from the terminal groups of the PEDOT chain, thus reducing the carrier concentration. Weak base imidazole with higher pK_b values is weakly de-doped for PEDOT:PSS. Furthermore, the removal of insulating PSS components and complex structural rearrangements occur together after base treatment, giving rise to enlarged grains and conductive domains of PEDOT, reducing the lamellar distances of alternating PEDOT and PSS simultaneously. This contributes to facilitating the carrier transport and then enhancing carrier mobility. Among the three bases, the imidazole-treated PEDOT:PSS film has a medium electrical conductivity (367 S cm^{-1}) while alleviating the acidity of PEDOT:PSS. Additionally, it also reduces equivalent series resistance, loss-angle tangent and enhances the lead capacitance ratio of aluminium electrolytic capacitors. Based on the mechanism proposed herein, we believe that our report provides a guideline for fabricating highly conductive, stable, and less corrosive PEDOT:PSS materials.

Data availability

The data that support the findings of this study are available from the corresponding authors upon reasonable request.

Author contributions

Piao Luo: conceptualization, methodology, investigation, data curation, visualization, writing–original draft. Kai Zhang: conceptualization, validation, supervision, writing – review & editing, resources, funding acquisition. Nanjie Wu, Shigui Peng, Lanlan Wei, Qiao Fan, and Tingting Luo, Yucheng Yin, Xiang Zhang: data curation, methodology, investigation, formal analysis, visualization. Yufei Liu, Min He, and Jie Yu: data curation, formal analysis, visualization, supervision. Shuhao Qin: conceptualization, supervision, resources, funding acquisition.

Conflicts of interest

There are no conflicts to declare.

Acknowledgements

This work was financially supported by the Guizhou Provincial Basic Research Program (Natural Science) (ZK[2024]613), the Guizhou Provincial Science and Technology Program Project Qiankehe Support [2023] General 415, and the Qiankehe Foundation-ZK[2023] General 084.

Notes and references

1 A. V. Volkov, K. Wijeratne, E. Mitraka, U. Ail, D. Zhao, K. Tybrandt, J. W. Andreasen, M. Berggren, X. Crispin and I. V. Zozoulenko, *Adv. Funct. Mater.*, 2017, **27**, 1700329.
2 Z. Zhu, Y. Bai, L. Wang, Y. Gao, X. Li, X. Yang and W. Lü, *Chem. Eng. J.*, 2024, **490**, 151587.
3 Y. Wang, S. S. Jia and Z. T. Zhang, *J. Mater. Chem. C*, 2023, **11**, 10435–10454.
4 X. Tang, X. Jin, Q. Zhang, Q. Zhao, Z. Yang and Q. Fu, *ACS Appl. Mater. Interfaces*, 2023, **15**, 23286–23298.
5 Z. Luo, C. Yang, X. Chen, W. Ma, S. Li and K. Fu, *J. Materiomics*, 2023, **9**, 438–446.
6 Z. Fan and J. Ouyang, *Adv. Electron. Mater.*, 2019, **5**, 1800769.
7 X. Fan, N. E. Stott, J. X. Zeng, Y. F. Li, J. Y. Ouyang, L. Chu and W. J. Song, *J. Mater. Chem. A*, 2023, **11**, 18561–18591.
8 Y. Li, Y. C. Pang, L. W. Wang, Q. Q. Li, B. G. Liu, J. M. Li, S. J. Liu and Q. Zhao, *Adv. Mater.*, 2024, **36**, 2310973.
9 L. Gang, H. Kaixi, D. Jue, G. Mengxue, C. Minkun, Z. Yuan and G. C. Fei, *Adv. Mater.*, 2022, **34**, 2200261.
10 R. Wan, J. Yu, Z. Quan, H. Ma, J. Li, F. Tian, W. Wang, Y. Sun, J. Liu, D. Gao, J. Xu and B. Lu, *Chem. Eng. J.*, 2024, **490**, 151454.
11 L. Zhao, C. Fang, B. Qin, X. Yang and P. Poechmueller, *Nano Energy*, 2024, **127**, 109772.
12 M. N. Gueye, A. Carella, J. Faure-Vincent, R. Demadrille and J.-P. Simonato, *Prog. Mater. Sci.*, 2020, **108**, 100616.
13 Y. S. Joo, H. Jeongdae, L. Hyeokjun, P. J. Tae, L. B. Hyung, J. K. In, Y. Anna and L. Y. Kyeung, *npj Flexible Electron.*, 2024, **8**, 22.
14 W. Wang, P. Guo, X. Liu, M. Chen, J. Li, Z. Hu, G. Li, Q. Chang, K. Shi, X. Wang and K. Lei, *Adv. Funct. Mater.*, 2024, **34**, 2316346.
15 Y. Huang, L. Tang and Y. Jiang, *CCS Chem.*, 2024, **6**, 1844–1867.
16 H. Kim, S. Nam and H. Lee, *J. Phys. Chem. C*, 2011, **115**, 13502–13510.
17 P. Tehrani, A. Kanciurzewska, X. Crispin, N. D. Robinson, M. Fahlman and M. Berggren, *Solid State Ionics*, 2006, **177**, 3521–3527.
18 Y. Wang, Y. Xu, J. Yun, Q. Cai, L. Zhai, D. Zhuang, G. Yang, H. Huang, M. Li, Y. Yang, L. Zhang and C. Zou, *Chem. Eng. J.*, 2024, **486**, 149964.
19 S. Chen, L. Song, Z. Tao, X. Shao, Y. Huang, Q. Cui and X. Guo, *Org. Electron.*, 2014, **15**, 3654–3659.
20 C. H. Hsieh, C. H. Huang, P. L. Chu, S. Y. Chu and P. Chen, *Org. Electron.*, 2021, **91**, 106081.
21 S. Kim, S. Y. Kim, M. H. Chung, J. Kim and J. H. Kim, *J. Mater. Chem. C*, 2015, **3**, 5859–5868.

22 Y. Wang, L. Yang, X. L. Shi, X. Shi, L. Chen, M. S. Dargusch, J. Zou and Z. G. Chen, *Adv. Mater.*, 2019, **31**, 1807916.
23 Y. Jiang, T. Liu and Y. Zhou, *Adv. Funct. Mater.*, 2020, **30**, 2006213.
24 P. Tan, F. Lu and Y. Han, *Chem. Mater.*, 2023, **35**, 6024–6038.
25 A. Cho, S. Kim, S. Kim, W. Cho, C. Park, F. S. Kim and J. H. Kim, *J. Polym. Sci., Part B: Polym. Phys.*, 2016, **54**, 1530–1536.
26 M. M. d. Kok, M. Buechel, S. I. E. Vulto, P. v. d. Weijer, E. A. Meulenkamp, S. H. P. M. d. Winter, A. J. G. Mank, H. J. M. Vorstenbosch, C. H. L. Weijtens and V. v. Elsbergen, *Phys. Status Solidi A*, 2004, **201**, 1342–1359.
27 F. Kong, C. Liu, H. Song, J. Xu, Y. Huang, H. Zhu and J. Wang, *Synth. Met.*, 2013, **185–186**, 31–37.
28 Y. Mochizuki, T. Horii and H. Okuzaki, *Trans. Mater. Res. Soc. Jpn.*, 2012, **37**, 307–310.
29 Y. C. Chin, M. Daboczi, C. Henderson, J. Luke and J.-S. Kim, *ACS Energy Lett.*, 2022, **7**, 560–568.
30 H. Yao, Z. Fan, P. Li, B. Li, X. Guan, D. Du and J. Ouyang, *J. Mater. Chem. A*, 2018, **6**, 24496–24502.
31 A. N. Aleshin, S. R. Williams and A. J. Heeger, *Synth. Met.*, 1998, **94**, 173–177.
32 S. S. Kalagi and P. S. Patil, *Synth. Met.*, 2016, **220**, 661–666.
33 Z. Fan, P. Li, D. Du and J. Ouyang, *Adv. Energy Mater.*, 2017, **7**, 1602116.
34 J. D. Morris and C. K. Payne, *Org. Electron.*, 2014, **15**, 1707–1710.
35 Z. Yan, Z. Song, Y. Tianhao, Z. Yan, Y. Guo, C. Han, H. Chengzhi, J. Wenchao, Z. Yu, L. Chunming, G. Xiaodan and L. Nan, *Nat. Commun.*, 2021, **12**, 4880.
36 Q. Fu, Y. Li, X. Wang, Q. Li, F. Wang and R. Yang, *J. Mater. Chem. C*, 2020, **8**, 17185–17193.
37 K. Z. Ullah, B. Olga, J. M. Javad, B. Robert, L. Xianjie, G. Roger, E. Thomas, E. D. R, A. J. W, F. Mats and C. Xavier, *J. Mater. Chem. C*, 2015, **3**, 10616–10623.
38 H. Mousavi, L. M. Ferrari, A. Whiteley and E. Ismailova, *Adv. Electron. Mater.*, 2023, **9**, 2201282.
39 Z. Li, L. Deng, H. Lv, L. Liang, W. Deng, Y. Zhang and G. Chen, *Adv. Funct. Mater.*, 2021, **31**, 2104836.
40 H. Yu, Z. Wu, X. Huang, S. Shi and Y. Li, *Org. Electron.*, 2018, **62**, 121–132.
41 M. Du, Y. Wen, Z. Chen, Y. Xu, J. Qin, H. Cheng, Y. Du, K. Zhang, S. Shin and J. Ouyang, *Adv. Funct. Mater.*, 2024, 2411815.
42 M. Culebras, C. M. Gomez and A. Cantarero, *J. Mater. Chem. A*, 2014, **2**, 10109–10115.
43 S. Garreau, G. Louarn, J. P. Buisson, G. Froyer and S. Lefrant, *Macromolecules*, 1999, **32**, 6807–6812.
44 J. Dong, J. Liu, X. Qiu, R. Chiechi, L. J. A. Koster and G. Portale, *Engineering*, 2021, **7**, 647–654.
45 J. Guo, K. Zhang, P. Luo, N. Wu, S. Peng, L. Wei, Y. Liu, M. He, J. Yu, S. Qin, Q. Fan, T. Luo and J. Xiao, *RSC Adv.*, 2024, **14**, 1602–1611.
46 A. Elschner, S. Kirchmeyer, W. Lovenich, U. Merker and K. Reuter, *PEDOT: Principles and Applications of an Intrinsically Conductive Polymer*, CRC Press, 2010.
47 Z. I. Kim D, *J. Phys. Chem. B*, 2019, **123**, 5160–5167.
48 S. Biswas, H. Kwon, K. C. Barsanti, N. Myllys, J. N. Smith and B. M. Wong, *Phys. Chem. Chem. Phys.*, 2020, **22**, 26265–26277.
49 S. Pezzola, M. Venanzi, V. Conte, F. Sabuzi and P. Galloni, *ChemPhysChem*, 2024, **25**, 202400550.
50 Y. Song, J. Tang, Y. Qi, J. Zhang, Y. Li and F. Wang, *Polymer*, 2023, **266**, 125649.
51 S. Nitin, K. Josef, M. A. K. Maurya, F. Giuseppino, O. Jan and M. B. Peter, *ACS Appl. Energy Mater.*, 2018, **1**, 336–342.
52 K. Dey, S. R. Chowdhury, E. Dykstra, A. Koronatov, H. P. Lu, R. Shinar, J. Shinar and P. Anzenbacher, *J. Mater. Chem. C*, 2020, **8**, 11988–11996.
53 K. Dey, S. Roy Chowdhury, E. Dykstra, H. P. Lu, R. Shinar, J. Shinar and P. Anzenbacher, Jr., *ACS Appl. Electron. Mater.*, 2021, **3**, 3365–3371.
54 N. Marques, S. Jana, M. J. Mendes, H. Águas, R. Martins and S. Panigrahi, *RSC Adv.*, 2024, **14**, 12397–12406.
55 X. Huang, L. Deng, F. Liu, Q. Zhang and G. Chen, *Energy Mater. Adv.*, 2021, **2021**, 1572537.
56 J. Dong, D. Gerlach, P. Koutsogiannis, P. Rudolf and G. Portale, *Adv. Electron. Mater.*, 2021, **7**, 2001284.
57 Q. Fan, K. Zhang, S. Peng, Y. Liu, L. Wei, S. Qin, M. He, J. Guo, T. Luo and J. Yu, *Prog. Org. Coat.*, 2024, **189**, 108308.
58 S. M. Kim, C. H. Kim, Y. Kim, N. Kim, W. J. Lee, E. H. Lee, D. Kim, S. Park, K. Lee, J. Rivnay and M. Yoon, *Nat. Commun.*, 2018, **9**, 3858.
59 L. Xin, Z. Ruike, L. Zhen, M. Jitendra, S. Ben, C. Yu, Q. Weiheng, Z. Zekun and Z. Peng, *npj Flexible Electron.*, 2022, **6**, 1–8.
60 M. Minakshi, A. Mujeeb, J. Whale, R. Evans, R. Aughterson, P. A. Shinde, K. Ariga and L. K. Shrestha, *ChemPlusChem*, 2024, **89**, 202400408.
61 M. Minakshi, A. Samayamanthry, J. Whale, R. Aughterson, P. A. Shinde, K. Ariga and L. Kumar Shrestha, *Chem.–Asian J.*, 2024, **19**, 202400622.
62 O. Inganäs, R. Erlandsson, C. Nylander and I. Lundström, *J. Phys. Chem. Solids*, 1984, **45**, 427–432.
63 S. Liu, J. An, Y. Li, J. Zhao, P. Qian, J. Jing and Y. Xu, *Adv. Eng. Mater.*, 2024, **26**, 2400926.